International Journal of Pavement Engineering
Vol. 12, No. 4, August 2011, 433–447

Taylor & Francis
Taylor & Francis Group

Numerical implementation and validation of a nonlinear viscoelastic and viscoplastic model for asphalt mixes

Chien-Wei Huang[a], Rashid K. Abu Al-Rub[a]*, Eyad A. Masad[a], Dallas N. Little[a] and Gordon D. Airey[b]

[a]*Zachry Department of Civil Engineering, Texas A&M University, College Station, TX 77845, USA;* [b]*Department of Civil Engineering, University of Nottingham, University Park, Nottingham, UK*

(*Received 16 March 2011; final version received 17 March 2011*)

This study presents the numerical implementation and validation of a constitutive model for describing the nonlinear behaviour of asphalt mixes. This model incorporates nonlinear viscoelasticity and viscoplasticity to predict the recoverable and irrecoverable responses, respectively. The model is represented in a numerical formulation and implemented in a finite element code using a recursive–iterative algorithm for nonlinear viscoelasticity and the radial return algorithm for viscoplasticity. Then the model is used to analyse the behaviour of asphalt mixtures subjected to single creep-recovery tests at different stress levels and temperatures. This experimental analysis includes the separation of the viscoelastic and viscoplastic strain components and identification of the material parameters associated with these components. Finally, the model is applied and verified against a set of creep-recovery tests at different stress levels and temperatures.

Keywords: nonlinear viscoelasticity; viscoplasticity; creep-recovery; finite element implementation; experimental validation

1. Introduction

Experimental measurements have shown that the response of hot mix asphalt (HMA) contains recoverable (viscoelastic) and irrecoverable (viscoplastic) deformation components (e.g. Perl *et al.* 1983, Sides *et al.* 1985, Collop *et al.* 2003). The recoverable response can be characterised as a nonlinear viscoelastic. The nonlinearity is caused by localised high-strain concentrations in the binder phase (Kose *et al.* 2000, Masad and Somadevan 2002). The Schapery's single integral model has been used in the past to describe the effect of stress and strain levels on the nonlinear viscoelastic behaviour of viscoelastic materials (e.g. Christensen 1968, Schapery 1969, 2000), and several numerical schemes of Schapery's theory have been developed and implemented using finite element (FE) to analyse the material viscoelastic response (e.g. Touati and Cederbaum 1997, 1998, Haj-Ali and Muliana 2004). Lee and Kim (1998) and Kim *et al.* (2007) have used a linear simplified form of the Schapery's viscoelastic model coupled with isotropic damage (Schapery 1991) to simulate the nonlinear behaviour of HMA. Sadd *et al.* (2004) employed the Schapery theory to represent the nonlinear viscoelastic behaviour of asphalt mixes and implemented it in a FE code using a recursive numerical scheme. Huang *et al.* (2007) implemented Schapery's nonlinear viscoelasticity model (Schapery 1969) in a FE code using the recursive–iterative numerical algorithm of Haj-Ali and Muliana (2004) to characterise the viscoelastic behaviour of HMA subjected to shear loading at different temperatures and strain levels.

The focus of this study is to expand the work by Huang *et al.* (2007) by including Perzyna's viscoplasticity theory for more accurate representation of the HMA mechanical behaviour. Perzyna's viscoplasticity theory (Perzyna 1971) has been used to describe the irrecoverable response of asphalt mixtures by several researchers. Seibi *et al.* (2001) developed an elasto-viscoplastic constitutive model for HMA. This model used the Perzyna's theory of viscoplasticity with the Drucker–Prager yield surface to model the irrecoverable component. However, this model used an elastic model to represent the recoverable component, which is not realistic for HMA especially at high-stress levels and high temperatures. Lu and Wright (1998) developed a model that employed Perzyna's viscoplasticity theory to represent the irrecoverable component of HMA, and considered the recoverable response as elastic or linear viscoelastic. Masad *et al.* (2005) developed an elasto-viscoplastic model with non-associated flow rule based on conventional Drucker–Prager yield surface for HMA. This model modified Perzyna's viscoplasticity to include material anisotropy and isotropic damage but with no viscoelasticity. Masad *et al.* (2007) improved this model by employing an extended Drucker–Prager yield surface which accounted for the influence of stress state (extension vs. compression) on material response, and implemented it in a FE programme. Nevertheless,

*Corresponding author. Email: rabualrub@civil.tamu.edu

ISSN 1029-8436 print/ISSN 1477-268X online

DOI: 10.1080/10298436.2011.574137
http://www.informaworld.com

surprisingly, these material constitutive models did not couple nonlinear viscoelasticity and viscoplasticity to predict the mechanical response of HMA, which is shown in this paper to be crucial at high-stress levels and high temperatures.

Therefore, the objectives of this research are to develop a general material constitutive model which integrates a nonlinear viscoelastic model with a viscoplastic model and to implement it into the FE code ABAQUS (2008) using a recursive–iterative numerical algorithm for viscoelasticity and return mapping algorithm for viscoplasticity. This study employs the Schapery's nonlinear viscoelastic model to represent the recoverable strain, whereas the viscoplastic strain is modelled using Perzyna's viscoplasticity theory. The model is used to analyse the experimental data on HMA mixtures subjected to creep-recovery tests at different temperatures and stress levels, and to verify the ability of the model to analyse asphalt mixtures response under the boundary conditions of laboratory tests.

The outline of this paper is as follows: In Section 2, a coupled nonlinear viscoelastic and viscoplastic model for analysing the recoverable (viscoelastic) and irrecoverable (viscoplastic) deformation components of asphalt concrete mixtures is presented. In Section 3, the numerical algorithms and computational implementation of the constitutive model in the FE code ABAQUS are presented in detail. The formulated model is calibrated and validated against a large set of experimental data on the creep-recovery response of HMA at different stress levels and different temperatures.

2. The nonlinear viscoelastic and viscoplastic model

Assuming small strain deformations, the total deformation of an asphalt concrete mix subjected to an applied stress can be decomposed into a recoverable component (i.e. viscoelastic) and an irrecoverable (i.e. viscoplastic) component such that:

$$\varepsilon_{ij} = \varepsilon_{ij}^{\mathrm{nve}} + \varepsilon_{ij}^{\mathrm{vp}}, \tag{1}$$

where ε_{ij} is the total strain tensor, $\varepsilon_{ij}^{\mathrm{nve}}$ is the nonlinear viscoelastic strain tensor and $\varepsilon_{ij}^{\mathrm{vp}}$ is the viscoplastic strain tensor.

2.1 *Nonlinear viscoelastic model*

This study employs the Schapery's nonlinear viscoelastic theory to model the recoverable component. The recoverable strain of Schapery integral form (1969) under an applied stress σ^{τ} is expressed as:

$$\varepsilon^{\mathrm{nve}}(t) = g_0 D_0 \sigma^t + g_1 \int_0^t \Delta D(\psi^t - \psi^{\tau}) \frac{d(g_2\sigma^{\tau})}{\mathrm{d}\tau}\mathrm{d}\tau, \tag{2}$$

where D_0 is the instantaneous elastic compliance, ΔD is the transient compliance, g_0, g_1 and g_2 are the nonlinear parameters related to stress or strain level and ψ^t is the reduced time which can be a function of stress/strain shift factor, temperature shift factor and other environment shift factors and is given by

$$\psi^t = \int_0^t \frac{d\xi}{a_{\mathrm{T}} a_{\mathrm{s}} a_{\mathrm{e}}}, \tag{3}$$

where a_{T} is the temperature shift factor, a_{s} is the strain or stress shift factor and a_{e} is the environment shift factor. For numerical convenience, this study uses the Prony series to represent the transient compliance ΔD as follows:

$$\Delta D^{\psi^t} = \sum_{n=1}^{N} D_n(1 - \exp(-\lambda_n \psi^t)), \tag{4}$$

where D_n is the nth coefficient of Prony series associated with the nth retardation time λ_n and N is the number of Prony series components. In the above equations, the superimposed t and τ designate the response at specific time.

The three-dimensional isotropic constitutive relations can be decoupled into deviatoric and volumetric parts presented as:

$$\varepsilon_{ij}^{\mathrm{nve}} = \frac{1}{2G} S_{ij} + \frac{\sigma_{kk}}{9K}\delta_{ij} = \frac{1}{2} J S_{ij} + \frac{1}{3} B \sigma_{kk}\delta_{ij}, \tag{5}$$

where G and K are the shear and bulk moduli, respectively, J and B are the shear and bulk compliances, respectively, S_{ij} is the deviatoric stress and σ_{kk} is the volumetric stress. Applying the Schapery's integral constitutive model in Equation (2), the deviatoric and volumetric strain components can be expressed, respectively, as follows (Lai and Bakker 1996):

$$\mathrm{e}_{ij}^{\mathrm{nve},t} = \frac{1}{2} g_0^t J_0 S_{ij}^t + \frac{1}{2} g_1^t \int_0^t \Delta J^{(\psi^t - \psi^{\tau})} \frac{d\left(g_2^{\tau} S_{ij}^{\tau}\right)}{\mathrm{d}\tau}\mathrm{d}\tau, \tag{6}$$

$$\varepsilon_{kk}^{\mathrm{nve},t} = \frac{1}{3} g_0^t B_0 \sigma_{kk}^t + \frac{1}{3} g_1^t \int_0^t \Delta B^{(\psi^t - \psi^{\tau})} \frac{d\left(g_2^{\tau} \sigma_{kk}^{\tau}\right)}{\mathrm{d}\tau}\mathrm{d}\tau, \tag{7}$$

where $\mathrm{e}_{ij}^{\mathrm{nve},t}$ is the deviatoric strain tensor and $\varepsilon_{kk}^{\mathrm{nve},t}$ is the volumetric strain tensor. The material constants J_0 and B_0 are the instantaneous elastic shear and bulk compliances, respectively.

Assuming Poisson's ratio υ to be time independent, the deviatoric strain $\mathrm{e}_{ij}^{\mathrm{nve},t}$ and volumetric strain $\varepsilon_{kk}^{\mathrm{nve},t}$ components can be expressed in terms of the hereditary integral formulation after substituting Equation (4) as

follows (Huang *et al.* 2007):

$$e_{ij}^{\mathrm{nve},t} = \frac{1}{2}\left[g_0^t J_0 + g_1^t g_2^t \sum_{n=1}^{N} J_n - g_1^t g_2^t \sum_{n=1}^{N} J_n \frac{1 - \exp(-\lambda_n \Delta\psi^t)}{\lambda_n \Delta\psi^t}\right] S_{ij}^t$$
$$- \frac{1}{2} g_1^t \sum_{n=1}^{N} J_n \left[\exp(-\lambda_n \Delta\psi^t) q_{ij,n}^{t-\Delta t} - g_2^{t-\Delta t} \frac{(1 - \exp(-\lambda_n \Delta\psi^t))}{\lambda_n \Delta\psi^t} S_{ij}^{t-\Delta t}\right], \quad (8),$$

$$\varepsilon_{kk}^{\mathrm{nve},t} = \frac{1}{3}\left[g_0^t B_0 + g_1^t g_2^t \sum_{n=1}^{N} B_n - g_1^t g_2^t \sum_{n=1}^{N} B_n \frac{1 - \exp(-\lambda_n \Delta\psi^t)}{\lambda_n \Delta\psi^t}\right] \sigma_{kk}^t$$
$$- \frac{1}{3} g_1^t \sum_{n=1}^{N} B_n \left[\exp(-\lambda_n \Delta\psi^t) q_{kk,n}^{t-\Delta t} - g_2^{t-\Delta t} \frac{(1 - \exp(-\lambda_n \Delta\psi^t))}{\lambda_n \Delta\psi^t} \sigma_{kk}^{t-\Delta t}\right]. \quad (9),$$

2.2 *Viscoplastic model*

This study uses an extended Drucker–Prager model with non-associated flow rule to model the viscoplastic strain. From Equation (1), the total strain rate $\dot{\varepsilon}_{ij}$ can be represented as

$$\dot{\varepsilon}_{ij} = \dot{\varepsilon}_{ij}^{\mathrm{nve}} + \dot{\varepsilon}_{ij}^{\mathrm{vp}}, \quad (10)$$

where $\dot{\varepsilon}_{ij}^{\mathrm{nve}}$ is the viscoelastic strain rate and $\dot{\varepsilon}_{ij}^{\mathrm{vp}}$ is the viscoplastic strain rate. This study uses Perzyna's model (Perzyna 1971) to present the viscoplastic strain rate component as

$$\dot{\varepsilon}_{ij}^{\mathrm{vp}} = \Gamma\langle\phi(f)\rangle \frac{\partial g}{\partial \sigma_{ij}}, \quad (11)$$

where Γ is the viscosity parameter, g is the viscoplastic potential energy function and ϕ is the overstress function which is expressed in terms of the yield surface f. In Equation (11), $\Gamma\langle\phi(f)\rangle$ is a positive scalar which determines the magnitude of viscoplastic strain rate $\dot{\varepsilon}_{ij}^{\mathrm{vp}}$, and $\partial g/\partial\sigma_{ij}$ is a vector which dominants the direction of $\dot{\varepsilon}_{ij}^{\mathrm{vp}}$. In addition, $\langle\cdot\rangle$ in Equation (11) is the McCauley bracket such that the following expression for ϕ can be postulated as

$$\langle\phi(f)\rangle = \begin{Bmatrix} 0 & \phi(f) \le 0 \\ \left(\frac{f}{\sigma_y^0}\right)^N & \phi(f) > 0 \end{Bmatrix}, \quad (12)$$

where σ_y^0 and N are the material constants. Equations (11) and (12) indicate that the viscoplasticity takes place only when the overstress function exceeds zero. To consider the effects of confinement, deviatoric stress and dilative behaviour of HMA, this study employs extended Drucker–Prager yield surface, which is presented in $I_1 - \tau$ plane as follows:

$$f = F(\sigma_{ij}) - \kappa\left(\varepsilon_{\mathrm{e}}^{\mathrm{vp}}\right) = \tau - \alpha I_1 - \kappa\left(\varepsilon_{\mathrm{e}}^{\mathrm{vp}}\right), \quad (13)$$

where α is the material parameter which is related to the material's internal friction. $\kappa\left(\varepsilon_{\mathrm{e}}^{\mathrm{vp}}\right)$ is an isotropic hardening function associated with the cohesive characteristics of the material and depends on the effective viscoplastic strain $\varepsilon_{\mathrm{e}}^{\mathrm{vp}}$, which is defined later. I_1 is the first stress invariant and τ is the deviatoric effective shear stress modified here to distinguish between the asphalt concrete behaviour under compression and extension (not necessarily tension) loading condition, such that (Tashman *et al.* 2005)

$$\tau = \frac{\sqrt{J_2}}{2}\left[1 + \frac{1}{d} + \left(1 - \frac{1}{d}\right)\frac{J_3}{\sqrt{J_2^3}}\right], \quad (14)$$

where $J_2 = 3S_{ij}S_{ij}/2$ and $J_3 = (9/2)S_{ij}S_{jk}S_{ki}$ are the second and third deviatoric stress invariants, respectively, and d is the material parameter which takes into account the distinction of asphalt concrete behaviour to compression and extension loading conditions. The range of d is from 0.778 to 1 (Masad *et al.* 2005). For uniaxial compression, the deviatoric effective shear stress $\tau = \sqrt{J_2}$, while $\tau = \sqrt{J_2}/d$ for uniaxial tension. A d less than 1 indicates that the material strength in compression is higher than the material strength in tension. If $d = 1$, the yield surface will become the Drucker–Prager yield surface.

The isotropic hardening function $\kappa\left(\varepsilon_{\mathrm{e}}^{\mathrm{vp}}\right)$ in Equation (13) is expressed as an exponential function of the effective viscoplastic strain $\varepsilon_{\mathrm{e}}^{\mathrm{vp}}$ following the work of Lemaitre and Chaboche (1990), such that

$$\kappa = \kappa_0 + \kappa_1\left\{1 - \exp\left(-\kappa_2\left(\varepsilon_{\mathrm{e}}^{\mathrm{vp}}\right)\right)\right\}, \quad (15)$$

where κ_0, κ_1 and κ_2 are the material parameters, which define the initial yield stress, the saturated yield stress and the strain-hardening rate, respectively. The effective viscoplastic strain rate $\dot{\varepsilon}_e^{vp}$ is expressed as (Dessouky 2005)

$$\dot{\varepsilon}_e^{vp} = \frac{\left(1-\frac{\beta}{3}\right)}{\sqrt{\left(1-\frac{\beta}{3}\right)^2+2\left(\frac{1}{2}+\frac{\beta}{3}\right)^2}}\sqrt{\dot{\varepsilon}_{ij}^{vp}\dot{\varepsilon}_{ij}^{vp}} = \frac{1}{\sqrt{1+2\left(\frac{\frac{1}{2}+\frac{\beta}{3}}{1-\frac{\beta}{3}}\right)^2}}\sqrt{\dot{\varepsilon}_{ij}^{vp}\dot{\varepsilon}_{ij}^{vp}}. \quad (16)$$

Several studies demonstrated that asphalt mixtures exhibit non-associated viscoplastic behaviour, which means that the direction of viscoplastic strain increment is not normal to the yield surface. The use of an associated flow rule (i.e. $g = f$) overestimates the dilation compared with experimental measurements (Masad *et al.* 2005, 2007). Hence, this study defines a viscoplastic potential function of a Drucker–Prager-type as in Equation (13) by replacing α with a smaller parameter β, such that

$$g = \tau - \beta I_1, \quad (17)$$

where β is the material parameter that describes the dilation or contraction behaviour of the material.

From Equation (17), $\partial g/\partial\sigma_{ij}$ in Equation (11) can be expressed as:

$$\frac{\partial g}{\partial \sigma_{ij}} = \frac{\partial \tau}{\partial \sigma_{ij}} - \frac{1}{3}\beta\delta_{ij}, \quad (18)$$

where δ_{ij} is the Kronecker delta and $\partial\tau/\partial\sigma_{ij}$ is given by

$$\frac{\partial \tau}{\partial \sigma_{ij}} = \frac{1}{2}\left[\frac{\frac{\partial J_2}{\partial \sigma_{ij}}}{2\sqrt{J_2}}\left(1+\frac{1}{d}\right) + \left(\frac{\frac{\partial J_3}{\partial \sigma_{ij}}J_2 - \frac{\partial J_2}{\partial \sigma_{ij}}J_3}{J_2^2}\right)\left(1-\frac{1}{d}\right)\right], \quad (19)$$

where $\partial J_2/\partial\sigma_{ij} = 3S_{ij}$ and $\partial J_3/\partial\sigma_{ij} = (27/2)S_{ik}S_{kj} - 3J_2\delta_{ij}$.

3. Numerical implementation

In this section, the time discretisation and numerical integration procedures for the presented nonlinear viscoelastic and viscoplastic model are presented. At the beginning of the step, by applying the given strain increment $\Delta\varepsilon_{ij} = \varepsilon_{ij}^{t+\Delta t} - \varepsilon_{ij}^{t}$ and knowing the values of the stress and internal variables from the previous step or time $t - \Delta t$, $(\cdot)^{t-\Delta t}$, the updated values at the end of the step or time t, $(\cdot)^t$, are obtained. Therefore, one can discretise the total strain in Equation (1), the effective viscoplastic strain in Equation (16) and the Cauchy stress tensor σ_{ij}, respectively, at the current time t as follows:

$$\varepsilon_{ij}^{t} = \varepsilon_{ij}^{nve,t} + \varepsilon_{ij}^{vp,t} = \varepsilon_{ij}^{t-\Delta t} + \Delta\varepsilon_{ij}^{t} = \varepsilon_{ij}^{nve,t-\Delta t} + \varepsilon_{ij}^{vp,t-\Delta t} + \Delta\varepsilon_{ij}^{nve,t} + \Delta\varepsilon_{ij}^{vp,t}, \quad (20)$$

$$\varepsilon_{e}^{vp,t} = \varepsilon_{e}^{vp,t-\Delta t} + \Delta\varepsilon_{e}^{vp,t}, \quad (21)$$

$$\sigma_{ij}^{t} = \sigma_{ij}^{t-\Delta t} + \Delta\sigma_{ij}^{t}. \quad (22)$$

The viscoelastic bulk and deviatoric strain increments can be expressed from Equations (8) and (9) as follows (Huang *et al.* 2007):

$$\begin{aligned}\Delta e_{ij}^{nve,t} &= e_{ij}^{nve,t} - e_{ij}^{nve,t-\Delta t} \\ &= \bar{J}^t S_{ij}^t - \bar{J}^{t-\Delta t} S_{ij}^{t-\Delta t} \\ &\quad - \frac{1}{2}\sum_{n=1}^{N} J_n\left[g_1^t \exp(-\lambda_n\Delta\psi^t) - g_1^{t-\Delta t}\right] q_{ij,n}^{t-\Delta t} \\ &\quad - \frac{1}{2} g_2^{t-\Delta t}\sum_{n=1}^{N} J_n\left\{ g_1^{t-\Delta t}\left[\frac{1-\exp(-\lambda_n\Delta\psi^{t-\Delta t})}{\lambda_n\Delta\psi^{t-\Delta t}}\right] \right. \\ &\quad \left. - g_1^t\left[\frac{1-\exp(-\lambda_n\Delta\psi^{t})}{\lambda_n\Delta\psi^{t}}\right]\right\} S_{ij}^{t-\Delta t},\end{aligned} \quad (23)$$

$$\begin{aligned}\Delta\varepsilon_{kk}^{nve,t} &= \varepsilon_{kk}^{nve,t} - \varepsilon_{kk}^{nve,t-\Delta t} = \bar{B}^t\sigma_{kk}^t - \bar{B}^{t-\Delta t}\sigma_{kk}^{t-\Delta t} \\ &\quad - \frac{1}{3}\sum_{n=1}^{N} B_n\left[g_1^t \exp(-\lambda_n\Delta\psi^t) - g_1^{t-\Delta t}\right] q_{kk,n}^{t-\Delta t} \\ &\quad - \frac{1}{3} g_2^{t-\Delta t}\sum_{n=1}^{N} B_n\left\{ g_1^{t-\Delta t}\left[\frac{1-\exp(-\lambda_n\Delta\psi^{t-\Delta t})}{\lambda_n\Delta\psi^{t-\Delta t}}\right] \right. \\ &\quad \left. - g_1^t\left[\frac{1-\exp(-\lambda_n\Delta\psi^{t})}{\lambda_n\Delta\psi^{t}}\right]\right\} \sigma_{kk}^{t-\Delta t},\end{aligned} \quad (24)$$

where the variables $q_{ij,n}^{t-\Delta t}$ and $q_{kk,n}^{t-\Delta t}$ are the shear and volumetric hereditary integrals for every Prony series term n at previous time step $t - \Delta t$, respectively. The hereditary integrals are updated at the end of every converged time increment, which will be used for the next time increment and are expressed as follows (Haj-Ali and Muliana 2004):

$$q_{ij,n}^{t} = \exp(-\lambda_n\Delta\psi^t) q_{ij,n}^{t-\Delta t} + \left(g_2^t S_{ij}^t - g_2^{t-\Delta t} S_{ij}^{t-\Delta t}\right) \times \frac{1-\exp(-\lambda_n\Delta\psi^t)}{\lambda_n\Delta\psi^t}, \quad (25)$$

$$q_{kk,n}^{t} = \exp(-\lambda_n\Delta\psi^t) q_{kk,n}^{t-\Delta t} + \left(g_2^t \sigma_{kk}^t - g_2^{t-\Delta t} \sigma_{kk}^{t-\Delta t}\right) \times \frac{1-\exp(-\lambda_n\Delta\psi^t)}{\lambda_n\Delta\psi^t}. \quad (26)$$

The increment of the viscoplastic strain in Equation (11) can be rewritten as follows:

$$\Delta\varepsilon_{ij}^{\mathrm{vp},t} = \Gamma\langle\phi(f)\rangle\frac{\partial g}{\partial\sigma_{ij}}\Delta t = \Delta\gamma^{\mathrm{vp},t}\frac{\partial g}{\partial\sigma_{ij}}, \tag{27}$$

where $\Delta\gamma^{\mathrm{vp},t}$ is the viscoplastic multiplier which is given by

$$\Delta\gamma^{\mathrm{vp},t} = \Delta t\Gamma\langle\phi(f)\rangle = \Delta t\Gamma\left(\frac{f\left(\sigma_{ij}^{t},\varepsilon_{\mathrm{e}}^{\mathrm{vp},t}\right)}{\sigma_{y}^{0}}\right)^{N}. \tag{28}$$

Substituting Equations (27) and (28) into Equation (21), the effective viscoplastic strain increment can be shown as

$$\begin{aligned}\varepsilon_{\mathrm{e}}^{\mathrm{vp},t} &= \varepsilon_{\mathrm{e}}^{\mathrm{vp},t-\Delta t} + \Delta\varepsilon_{\mathrm{e}}^{\mathrm{vp},t}\\ &= \varepsilon_{\mathrm{e}}^{\mathrm{vp},t-\Delta t} + \frac{\Delta\gamma^{\mathrm{vp},t}}{\sqrt{1+2\left(\frac{\frac{1}{2}+\frac{\beta}{3}}{1-\frac{\beta}{3}}\right)^{2}}}\sqrt{\frac{\partial g}{\partial\sigma_{ij}}\frac{\partial g}{\partial\sigma_{ij}}}.\end{aligned} \tag{29}$$

The coupled nonlinear viscoelastic and viscoplastic algorithm starts at a trial stress, which is assumed to be viscoelastic and decomposed into deviatoric and volumetric components such that their increments can be expressed as follows [see Huang *et al.* (2007)]:

$$\Delta S_{ij}^{t,\mathrm{tr}} = \frac{1}{\bar{J}^{t,\mathrm{tr}}}\left\{\Delta\mathrm{e}_{ij}^{t} + \frac{1}{2}g_{1}^{t,\mathrm{tr}}\sum_{n=1}^{N}J_{n}\left[\exp\left(-\lambda_{n}\Delta\psi^{t}\right)-1\right]q_{ij,n}^{t-\Delta t}\right\}, \tag{30}$$

$$\Delta\sigma_{kk}^{t,\mathrm{tr}} = \frac{1}{\bar{B}^{t,\mathrm{tr}}}\left\{\Delta\varepsilon_{kk}^{t} + \frac{1}{3}g_{1}^{t,\mathrm{tr}}\sum_{n=1}^{N}B_{n}\left[\exp\left(-\lambda_{n}\Delta\psi^{t}\right)-1\right]q_{kk,n}^{t-\Delta t}\right\}. \tag{31}$$

Once the trial stress exceeds the yield limit, the calculation of the viscoplastic strain increment is carried out; otherwise, the total stress and strain are viscoelastic.

According to Wang *et al.* (1997), one can define a consistency condition for rate-dependent plasticity (viscoplasticity) similar to rate-independent plasticity theory such that a dynamic (rate-dependent) yield surface, χ, can be expressed from Equations (11)–(13) as follows:

$$\chi = \tau - \alpha I_{1} - \kappa\left(\varepsilon_{\mathrm{e}}^{\mathrm{vp}}\right) - \sigma_{y}^{0}\left(\frac{\dot{\gamma}^{\mathrm{vp}}}{\Gamma}\right)^{1/N} \le 0, \tag{32}$$

such that the above dynamic yield surface satisfies the Kuhn–Tucker loading–unloading conditions (consistency)

$$\chi \le 0; \quad \dot{\gamma}^{\mathrm{vp}} \ge 0; \quad \dot{\gamma}^{\mathrm{vp}}\chi = 0; \quad \dot{\chi} = 0. \tag{33}$$

A trial dynamic yield surface function χ^{tr} can be defined from Equation (32) as

$$\begin{aligned}\chi = \tau^{\mathrm{tr}} &- \alpha I_{1}^{\mathrm{tr}} - \kappa\left(\left(\varepsilon_{\mathrm{e}}^{\mathrm{vp},t-\Delta t}\right)\right)\\ &- \sigma_{y}^{0}\left(\frac{\Delta\gamma^{\mathrm{vp},t-\Delta t}}{\Delta t\Gamma}\right)^{1/N}.\end{aligned} \tag{34}$$

To calculate $\varepsilon_{\mathrm{e}}^{\mathrm{vp},t}$, one can iteratively calculate $\Delta\gamma^{\mathrm{vp},t}$ through using the Newton–Raphson scheme. Once one obtains $\Delta\gamma^{\mathrm{vp},t}$, the viscoplastic strain increment $\Delta\varepsilon_{ij}^{\mathrm{vp}}$ can be calculated from Equation (27). In the Newton–Raphson scheme, the differential of χ with respect to $\Delta\gamma^{\mathrm{vp}}$ is needed and can be expressed as follows:

$$\frac{\partial\chi}{\partial\Delta\gamma^{\mathrm{vp}}} = -\frac{\partial\kappa}{\partial\Delta\varepsilon_{\mathrm{e}}^{\mathrm{vp}}}\frac{\partial\Delta\varepsilon_{\mathrm{e}}^{\mathrm{vp}}}{\partial\Delta\gamma^{\mathrm{vp}}} - \frac{\sigma_{y}^{0}}{\Delta\gamma^{\mathrm{vp}}N}\left(\frac{\Delta\gamma^{\mathrm{vp}}}{\Delta t\Gamma}\right)^{\frac{1}{N}}. \tag{35}$$

At the $(k+1)$ iteration, the viscoplastic multiplier is calculated by

$$\left(\Delta\gamma^{\mathrm{vp},t}\right)^{k+1} = \left(\Delta\gamma^{\mathrm{vp},t}\right)^{k} - \left[\left(\frac{\partial\chi}{\partial\Delta\gamma^{\mathrm{vp},t}}\right)^{k}\right]^{-1}\chi^{k}. \tag{36}$$

Because both the nonlinear viscoelastic and viscoplastic strain increments are the functions of current stress, this study employs the recursive–iteration algorithm with the Newton–Raphson method to obtain the current stress and the updated values of the viscoelastic and viscoplastic strain increments by minimising the residual strain defined as

$$R_{ij}^{t} = \Delta\varepsilon_{ij}^{\mathrm{nve},t} + \Delta\varepsilon_{ij}^{\mathrm{vp},t} - \Delta\varepsilon_{ij}^{t}. \tag{37}$$

This algorithm applies iterations at both the material and the structure levels to minimise the error; otherwise, very small increments are required. The stress increment at the $(k+1)$ iteration is calculated by

$$\left(\Delta\sigma_{ij}^{t}\right)^{k+1} = \left(\Delta\sigma_{ij}^{t}\right)^{k} - \left[\left(\frac{\partial R_{ij}^{t}}{\partial\sigma_{kl}^{t}}\right)^{k}\right]^{-1}\left(R_{kl}^{t}\right)^{k}, \tag{38}$$

where the differential of R_{ij}^{t} gives the consistent tangent compliance, which can be derived as follows:

$$\frac{\partial R_{ij}^{t}}{\partial\sigma_{kl}} = \frac{\partial\Delta\varepsilon_{ij}^{\mathrm{nve},t}}{\partial\sigma_{kl}} + \frac{\partial\Delta\varepsilon_{ij}^{\mathrm{vp},t}}{\partial\sigma_{kl}}, \tag{39}$$

where $\partial\Delta\varepsilon_{ij}^{\mathrm{nve}}/\partial\sigma_{kl}$ is the nonlinear viscoelastic tangent compliance which is derived in Huang *et al.* (2007). Whereas the viscoplastic tangent compliance is derived

from Equations (13), (27), and (28), such that

$$\frac{\partial \Delta\varepsilon_{ij}^{\mathrm{vp},t}}{\partial\sigma_{kl}} = \frac{\partial g}{\partial\sigma_{ij}}\frac{\partial \Delta\gamma^{\mathrm{vp},t}}{\partial\sigma_{kl}} + \Delta\gamma^{\mathrm{vp},t}\frac{\partial^2 g}{\partial\sigma_{ij}\partial\sigma_{kl}}$$
$$= \frac{\Delta t\Gamma N}{\sigma_y^0}\left(\frac{f}{\sigma_y^0}\right)^{N-1}\frac{\partial g}{\partial\sigma_{ij}}\frac{\partial f}{\partial\sigma_{kl}}$$
$$+ \Delta t\Gamma\left(\frac{f}{\sigma_y^0}\right)^{N}\frac{\partial^2 g}{\partial\sigma_{ij}\partial\sigma_{kl}}, \quad (40)$$

where $\partial^2 g/\partial\sigma_{ij}\partial\sigma_{kl}$ is given by

$$\frac{\partial^2\tau}{\partial\sigma_{ij}\partial\sigma_{kl}} = 1.5\left(\delta_{ik}\delta_{jl} - \frac{1}{3}\delta_{ij}\delta_{kl}\right)\left[\frac{1+1/d}{2\sqrt{J_2}} - \frac{J_3(1-1/d)}{J_2^2}\right]$$
$$+ 1.5S_{kl}\left[\frac{-\frac{\partial J_2}{\partial\sigma_{ij}}(1+1/d)J_2^{-1.5}}{4}\right.$$
$$\left.+(1-1/d)\left(2J_3J_2^{-3}\frac{\partial J_2}{\partial\sigma_{ij}} - J_2^{-2}\frac{\partial J_3}{\partial\sigma_{ij}}\right)\right]$$
$$+ \frac{(1-1/d)}{2J_2^2}\left[\frac{27(\delta_{ik}S_{lj}+\delta_{jl}S_{ik})}{2} - 9(\delta_{kl}S_{ij}+\delta_{ij}S_{kl})\right]$$
$$- \left(\frac{27}{4}S_{km}S_{ml} - 1.5J_2S_{kl}\right)\left[\frac{(1-1/d)\frac{\partial J_2}{\partial\sigma_{ij}}}{J_2^2}\right]. \quad (41)$$

If the stress does not exceed the yield limit, the material compliance will only be the nonlinear viscoelastic compliance $\partial\Delta\varepsilon_{ij}^{\mathrm{nve}}/\partial\sigma_{kl}$; otherwise, the material compliance will be a coupled nonlinear viscoelastic and viscoplastic one. The nonlinear viscoelastic and viscoplastic algorithm is shown in Figure 1. The flowchart of viscoplastic strain increment calculation using the Newton–Raphson method is shown in Figure 2.

4. Calibration, application and validation

In this section, the computational constitutive model is calibrated and validated by analysing a set of experimental data for an asphalt mixture, which was tested using different stress levels and temperatures. The asphalt is referred to as 10 mm Dense Bitumen Macadam, which is a continuously graded mixture with asphalt binder content of 5.5%. Granite aggregate and asphalt binder with a penetration grade of 70/100 were used in preparing this asphalt mixture. Cylindrical specimens with a diameter of 100mm and a height of 100mm were compacted using the gyratory compactor (Grenfell *et al.* 2008).

Single creep-recovery tests are conducted over a range of temperatures and stress levels. The test conditions are summarised in Table 1. This test applies a constant step-loading and then removes the loading until the rate of recovered deformation during the relaxation period is approximately zero. The load is held for different loading times (LT), and the response is recorded for each LT as shown in Table 1. An example of experimental measurements at a temperature of 20°C is shown in Figure 3. The details about the experimental results are given in the work of Grenfell *et al.* (2008).

4.1 *Separation of recoverable and irrecoverable components and identification of the viscoelastic material parameters*

The first step of the following experimental analysis is to separate the recoverable (viscoelastic) and irrecoverable (viscoplastic) components. A schematic of a single creep-recovery test is shown in Figure 4 for a constant stress loading and unloading condition. Hence, one can express the creep and relaxation strains for a constant stress from Equations (1) and (2) as follows:

$$\varepsilon^{\mathrm{c}}(t) = \varepsilon^{\mathrm{rec}}(t) + \varepsilon^{\mathrm{irrec}}(t) = g_1g_2\sigma\Delta D(t) + \varepsilon^{irrec}(t), \quad (42)$$

$$\varepsilon^{r}(t) = \varepsilon^{\mathrm{rec}}(t) + \varepsilon^{\mathrm{irrec}}(t_a)$$
$$= [g_2\sigma\Delta D(t) - g_2\sigma\Delta D(t-t_a)] + \varepsilon^{irrec}(t_a), \quad (43)$$

where ε^{c} is the total creep strain, ε^{r} is the total relaxation strain, $\varepsilon^{\mathrm{rec}}$ is the recoverable strain, $\varepsilon^{\mathrm{irrec}}$ is the irrecoverable strain and t_a is the LT as shown in Figure 4. When the nonlinear parameters g_1 and g_2 are equal to unity, Equations (42) and (43) reduce to the linear viscoelastic case.

Saadeh *et al.* (2007) have shown that the identification of the instantaneous strain response and its separation from the time-dependent strain response is highly dependent on the experimental setup and on the selection of the time threshold that marks the end of what is considered 'instantaneous' response. Therefore, it was decided in this study to consider the entire recoverable strain component as time-dependent such that one can set the instantaneous strain $g_0D_0\sigma$ to be equal to zero.

The first step of the analysis procedure is to obtain the Prony series coefficients D_n and λ_n in Equation (4) from a linear viscoelastic response at low-stress levels and low temperatures. However, in this study, it is assumed that the recoverable response is linear viscoelastic ($g_1 = g_2 = 1$) at the lowest stress level as shown in Table 1 of each considered temperature. The analysis employs the strain $\Delta\varepsilon^{r1}$ as shown in Figure 4, which is the recovered strain between t_a and t_b to obtain the Prony series coefficients D_n and λ_n at the lowest stress level (linear viscoelastic case). The expression for $\Delta\varepsilon^{r1}(t)$ can be derived from Equations (42) and (43), such that

$$\Delta\varepsilon^{r1}(t) = \varepsilon^{\mathrm{c}}(t_a) - \varepsilon^{r}(t)$$
$$= \sigma\left\{\begin{array}{l}\sum_{n=1}^{N} D_n[1 - \exp(-\lambda_n t_a)] - \\ \sum_{n=1}^{N} D_n[1 - \exp(-\lambda_n t)] \\ \quad + \sum_{n=1}^{N} D_n[1 - \exp(-\lambda_n(t-t_a))]\end{array}\right\}, \quad (44)$$

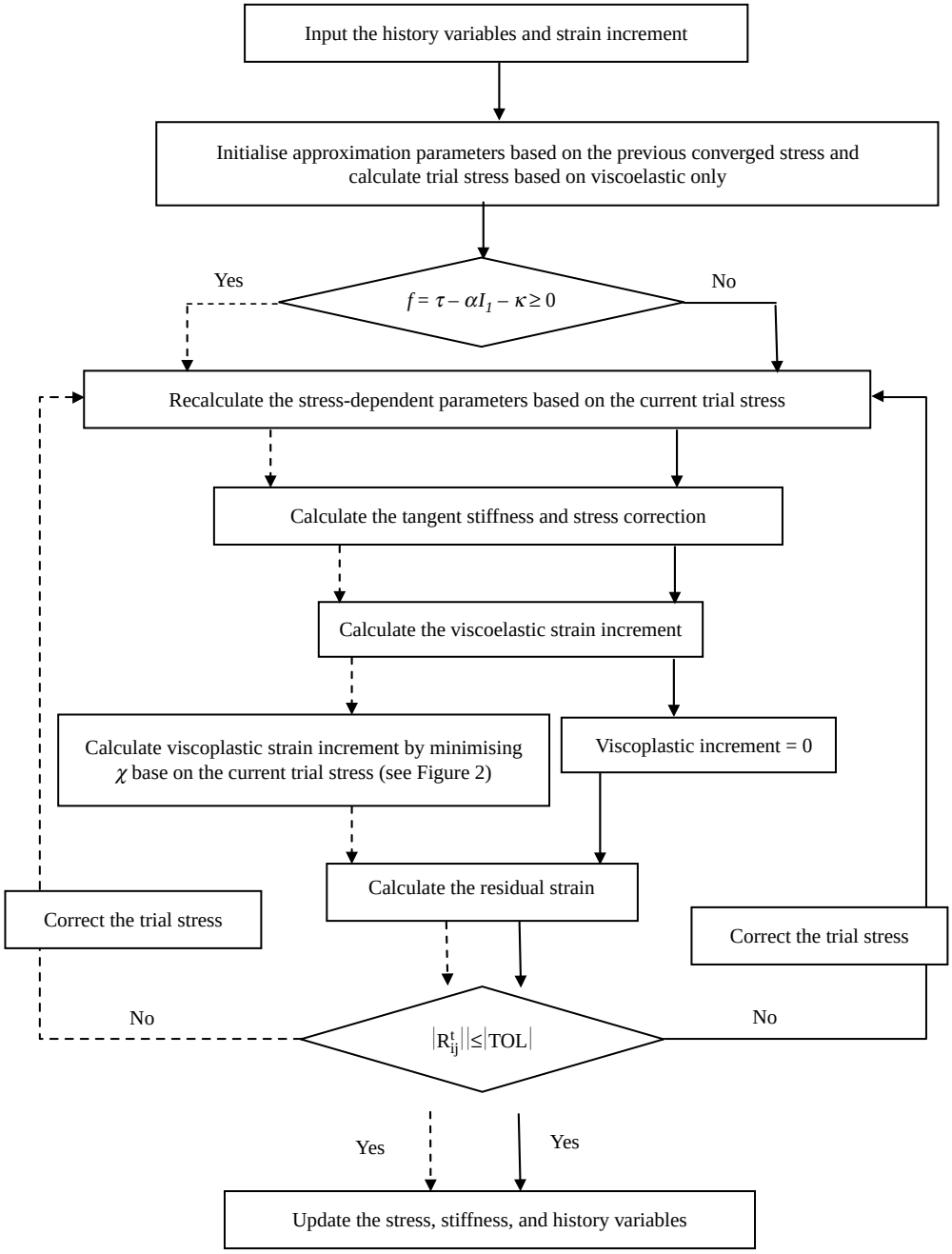

Figure 1. The flowchart of nonlinear viscoelastic and viscoplastic implementation.

Then the Prony series coefficients are determined by minimising the error between the measurements of $\Delta\varepsilon^{r1}(t)$ and Equation (44). The values of D_n and λ_n at different temperatures are listed in Table 2. The nonlinear viscoelastic expressions in Equations (42) and (43) with D_n and λ_n shown in Table 2 can then be used to analyse the experimental measurements at higher stress levels to determine the nonlinear viscoelastic parameters g_1 and g_2. At the higher stress levels, the following expression for the recovered strain $\Delta\varepsilon^{r3}(t)$ from $t = t_1$ to $t = t_b$ (see Figure 4) can be derived from Equation (43) and then used to determine the nonlinear parameter g_2, such that:

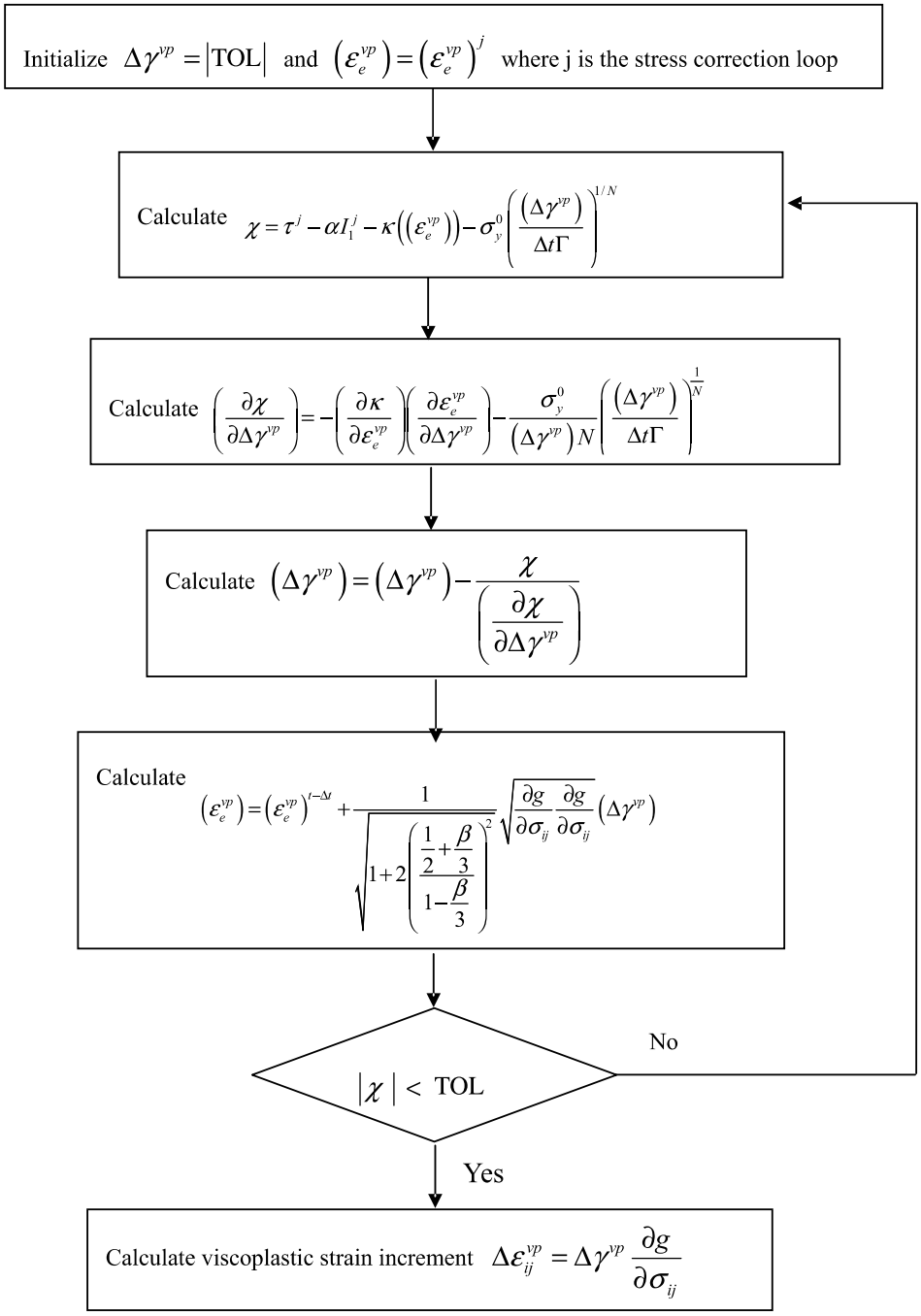

Figure 2. The flowchart of Newton–Raphson method for viscoplastic strain increments.

$$\Delta\varepsilon^{r3}(t) = \varepsilon^r(t_1) - \varepsilon^r(t) = g_2\sigma\left\{\begin{array}{l}\sum_{n=1}^{N} D_n[1 - \exp(-\lambda_n t_1)] \\ \quad + \sum_{n=1}^{N} D_n[1 - \exp(-\lambda_n(t_1 - t_a))] \\ -\sum_{n=1}^{N} D_n[1 - \exp(-\lambda_n t)] \\ \quad + \sum_{n=1}^{N} D_n[1 - \exp(-\lambda_n(t - t_a))]\end{array}\right\}. \quad (45)$$

Table 1. Summary of test conditions.

Temperature (°C)	Stress level (kPa) and	Loading time (sec)
10	2000	400, 600
10	2500	300, 350
20	1000	40, 210, 1517
20	1500	30, 150, 420
40	500	130, 180
40	750	50

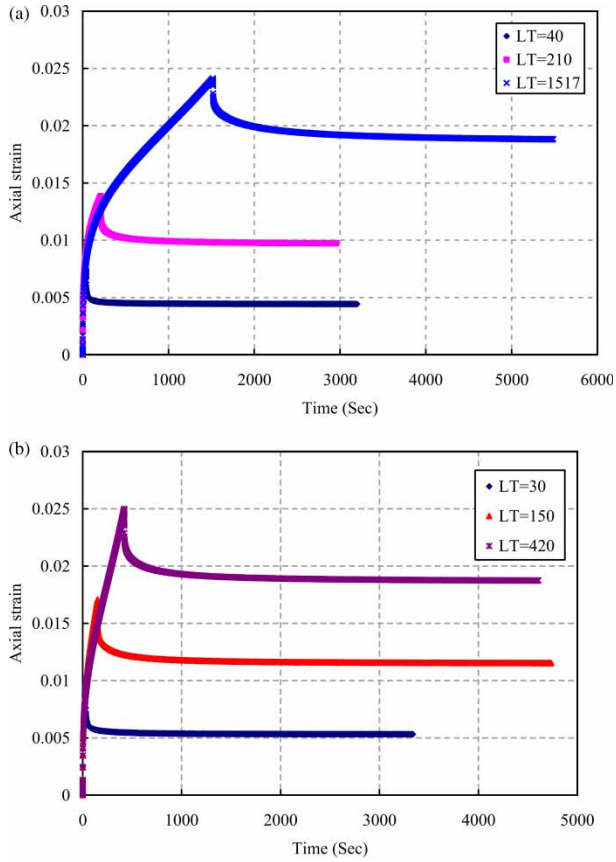

Figure 3. The experimental measurements at a temperature 20°C for stress levels: (a) 1000 kPa and (b) 1500 kPa (LT indicates loading times in seconds).

Once the nonlinear parameter g_2 is obtained, the expression for the recovered strain $\Delta\varepsilon^{r2}(t)$ which can be derived from Equations (42) and (43) is fitted to the experimental measurements from $t = t_a$ to $t = t_1$ (see Figure 4) to obtain the nonlinear parameter g_1, such that

$$\Delta\varepsilon^{r2}(t) = \varepsilon^{c}(t_a) - \varepsilon^{r}(t) = \sigma\left\{\begin{array}{l} g_1 g_2 \sum_{n=1}^{N} D_n\left[1 - \exp\left(-\lambda_n t_a\right)\right] \\ -g_2 \sum_{n=1}^{N} D_n[1 - \exp\left(-\lambda_n t\right)] \\ \quad +g_2 \sum_{n=1}^{N} D_n[1 - \exp\left(-\lambda_n (t - t_a)\right)] \end{array}\right\}. \tag{46}$$

The nonlinear parameters at different temperatures are listed in Table 3. Once the Prony series coefficients (Table 2) and the nonlinear parameters (Table 3) are obtained, the nonlinear recoverable (viscoelastic) strain in Equations (42) and (43) can be calculated. Consequently, the irrecoverable (viscoplastic) strain can be obtained by subtracting the viscoelastic strain from the total strain. For example, the decoupled viscoelastic and viscoplastic responses are shown in Figure 5 for two stress levels at a temperature of 20°C.

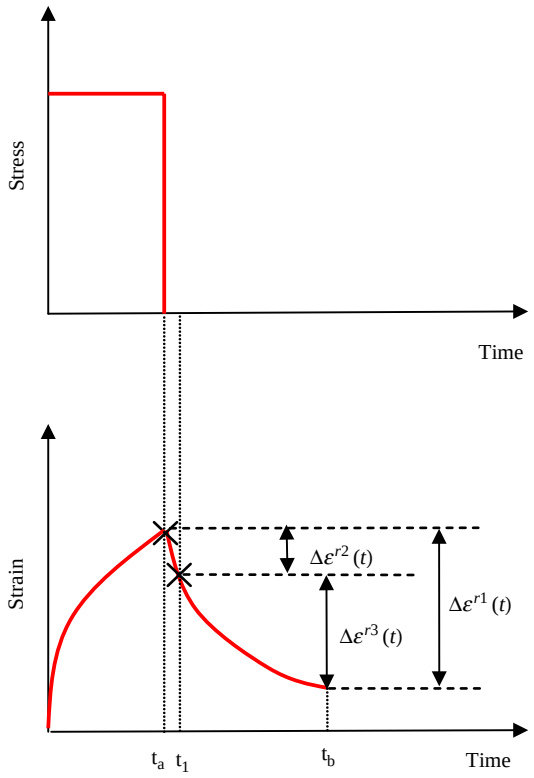

Figure 4. A schematic of single creep-recovery test.

4.2 *Determination of the viscoplastic parameters*

Once the viscoplastic strain is separated from the viscoelastic strain as shown in the previous section, one can then identify the material constants associated with the viscoplasticity equations as shown here. The dynamic yield surface in Equation (32) for a uniaxial compression step-loading is expressed as:

$$\begin{aligned} \chi &= \sigma_1 - \alpha\frac{\sigma_1}{3} - \kappa\left(\varepsilon_e^{vp,t}\right) - \sigma_y^0\left(\frac{\Delta\gamma^{vp,t}}{\Delta t\Gamma}\right)^{1/N} \\ &= \sigma_1 - \alpha\frac{\sigma_1}{3} - \left[\kappa_0 + \kappa_1\left(1 - \exp\left(-\kappa_2\varepsilon_e^{vp}\right)\right)\right] \\ &\quad - \sigma_y^0\left(\frac{\Delta\gamma^{vp,t}}{\Delta t\Gamma}\right)^{1/N} \cong 0, \end{aligned} \tag{47}$$

Table 2. The Prony series coefficients.

		Linear viscoelastic material coefficients		
		Temp = 10°C	20°C	40°C
n	λ_n (S^{-1})	D_n (MPa^{-1})	D_n (MPa^{-1})	D_n (MPa^{-1})
1	10	7.81×10^{-7}	1.98×10^{-7}	3.98×10^{-6}
2	1	0.0	1.48×10^{-6}	0.0
3	0.1	5.42×10^{-7}	6.56×10^{-7}	1.55×10^{-6}
4	0.01	5.58×10^{-7}	1.43×10^{-6}	6.77×10^{-7}
5	0.001	1.62×10^{-6}	2.74×10^{-6}	6.05×10^{-8}

Table 3. The values of the nonlinear viscoelastic parameters at different temperatures.

Nonlinear viscoelastic parameters	Temperature (°C)		
	10	20	40
g_1	0.908	1.194	0.576
g_2	1.017	0.837	1.920

where σ_1 is the applied uniaxial compressive stress. By rearranging Equation (47), one can write

$$\frac{\Delta\gamma^{vp,t}}{\Delta t} = \Gamma\left[\frac{\left\{\sigma_1 - \alpha\frac{\sigma_1}{3} - \left[\kappa_0 + \kappa_1\left(1 - \exp\left(-\kappa_2\varepsilon_e^{vp}\right)\right)\right]\right\}}{\sigma_y^0}\right]^N, \tag{48}$$

where $\Delta\gamma^{vp,t}$ can be obtained from the separated $\Delta\varepsilon_1^{vp,t}$ from the experimental measurements for uniaxial compressive stress using the following expression obtained from Equation (27), such that

$$\Delta\gamma^{vp,t} = \frac{\Delta\varepsilon_1^{vp,t}}{\frac{\partial g}{\partial\sigma_1}} = \frac{\Delta\varepsilon_1^{vp,t}}{\left(1 - \frac{\beta}{3}\right)}, \tag{49}$$

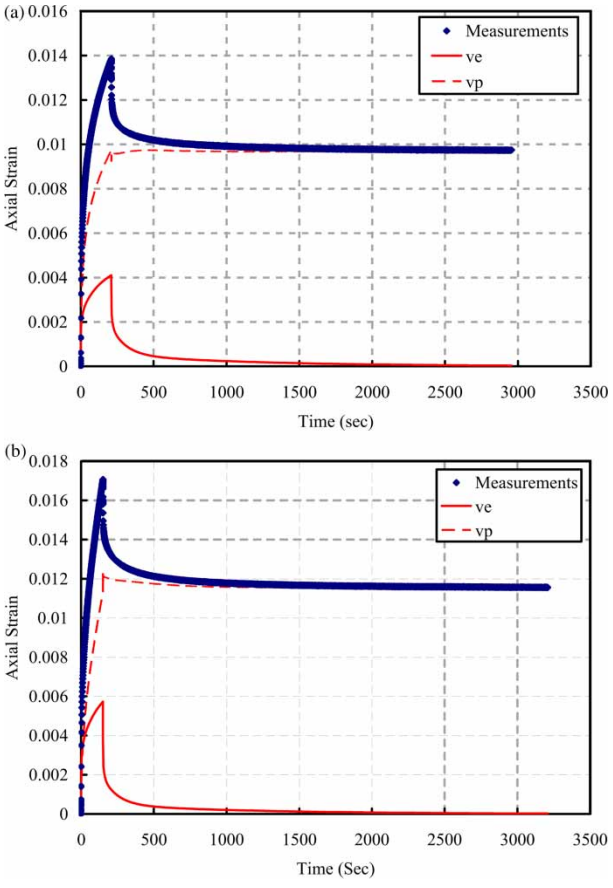

Figure 5. An example of separation of the viscoelastic and viscoplastic strains at a temperature of 20°C for stress levels: (a) 1000 kPa and (b) 1500 kPa.

Table 4. The values of the viscoplastic parameters at different temperatures.

Viscoplastic parameters	Temperature (°C)		
	10	20	40
α	0.35	0.30	0.25
β	0.10	0.15	0.20
Γ	4.0×10^{-4}	5.0×10^{-4}	1.0×10^{-2}
N	3.63	3.63	3.63
κ_0	40	35	10
κ_1	930	610	550
κ_2	270	215	160

where $\Delta\varepsilon_1^{vp,t}$ is the axial viscoplastic strain increment. Moreover, ε_e^{vp} can be calculated from Equation (29) for uniaxial compression as

$$\varepsilon_e^{vp} = \frac{1}{\sqrt{1 + 2\left(\frac{0.5+\beta/3}{1-\beta/3}\right)^2}}\sqrt{\left(\varepsilon_1^{vp}\right)^2 + 2\left(\varepsilon_2^{vp}\right)^2}, \tag{50}$$

where ε_1^{vp} and ε_2^{vp} are the viscoplastic strains in the axial and radial directions, respectively. However, as the experimental

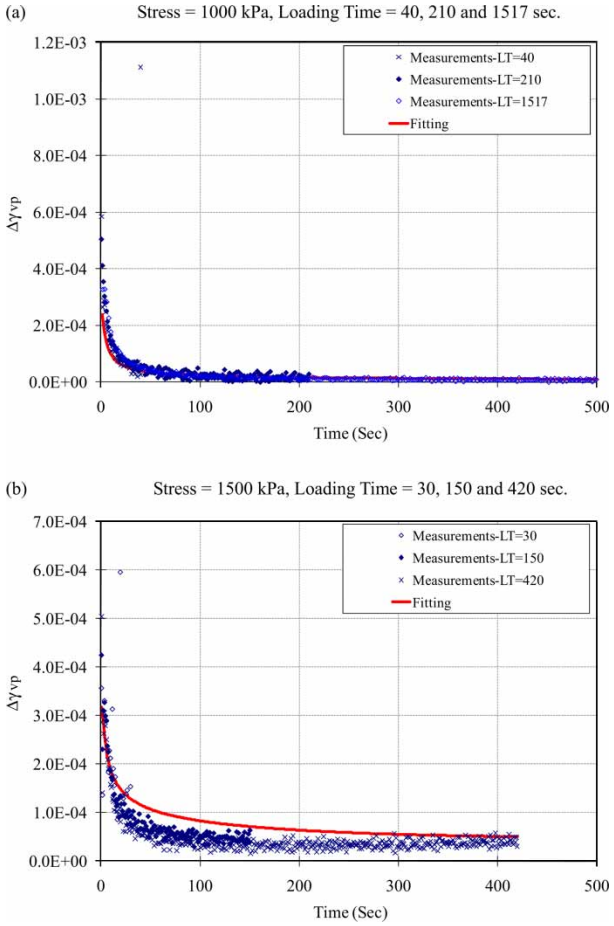

Figure 6. The viscoplastic fitting procedure of $\Delta\gamma^{vp}$ at a temperature of 20°C.

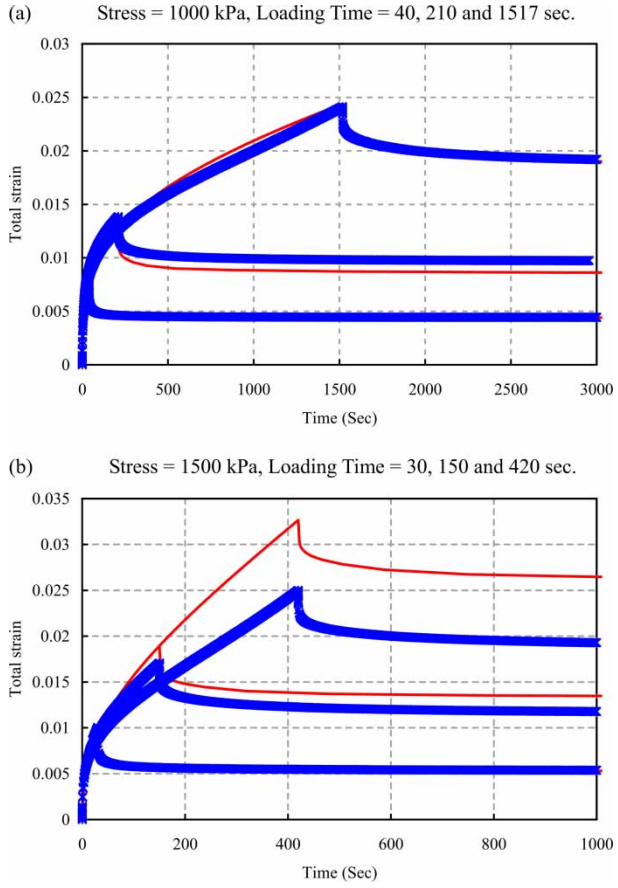

Figure 7. The comparison of total strain between measurements and model predictions at a temperature of 20°C.

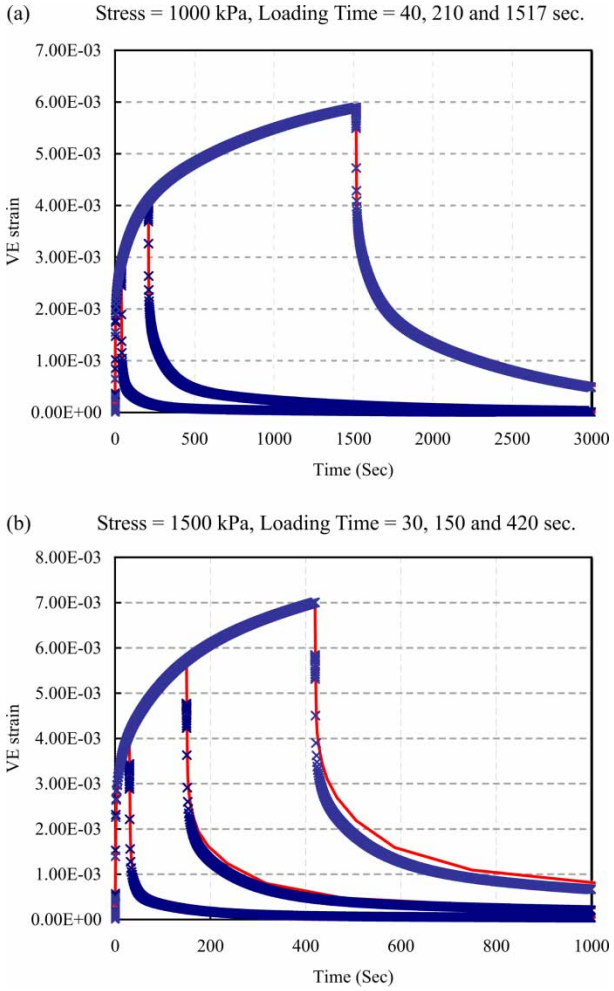

Figure 8. The comparison of viscoelastic strain between decoupled measurements and model predictions at a temperature of 20°C.

measurements did not include ε_2^{vp}, this study calculates ε_2^{vp} from the following relation between the axial and radial viscoplastic strains. The relation between the axial and the radial viscoplastic strains for uniaxial compression can be determined from Equation (11) as

$$\frac{\varepsilon_2^{vp}}{\varepsilon_1^{vp}} = \frac{-\partial g/\partial \sigma_{22}}{\partial g/\partial \sigma_{11}} \Rightarrow \varepsilon_2^{vp} = \frac{0.5+\beta/3}{1-\beta/3}\varepsilon_1^{vp}, \quad (51)$$

Once $\Delta\gamma^{vp,t}$ and ε_e^{vp} are calculated from the analysed experimental viscoplastic strain data using Equations (49) and (50), the viscoplastic parameters Γ, N, κ_0, κ_1 and κ_2 can be obtained by minimising the error between the measurements and Equation (48).

As the yield surface parameter α changes only slightly at small strain levels (Seibi *et al.* 2001), α is assumed here to be constant. The parameter β is also assumed to have a value less than α, because using $\alpha \geq \beta$ would result in higher dilation than is obtained from experimental measurements (Masad *et al.* 2007). Therefore, the values of α and β are assumed to be a constant at a given temperature. The parameter β is assumed to increase with temperature as asphalt mixtures dilate more as temperature increases. The α and β values are listed in Table 4. Furthermore, it is found that σ_y^0 is stress dependent and follows $\sigma_y^0 = \sigma_1(1-\alpha/3)$ which is used to obtain the viscoplastic parameters such that Equation (48) can be rewritten as follows:

$$\frac{\Delta\gamma^{vp,t}}{\Delta t} = \Gamma\left[1 - \frac{\left[\kappa_0 + \kappa_1\left(1 - \exp\left(-\kappa_2\varepsilon_e^{vp}\right)\right)\right]}{\sigma_1 - \alpha\frac{\sigma_1}{3}}\right]^N. \quad (52)$$

The advantages of the above analysis procedure are (1) fitting the material response at different stress levels simultaneously; (2) normalising the overstress function, which represents the distance between the current stress and the yield surface over a scale between 0 and 1, such that Γ is used then to determine the magnitude of viscoplastic increment and (3) incorporating the applied stress effect within the dynamic yield surface. The fitting for both stress levels at a temperature of 20°C is shown in

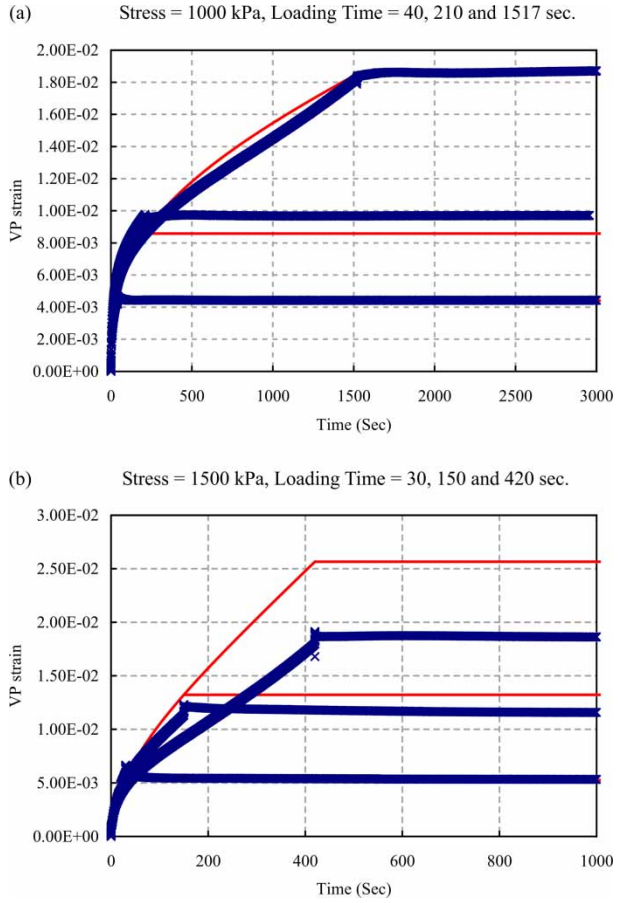

Figure 9. The comparison of viscoplastic strain between decoupled measurements and model predictions at a temperature of 20°C.

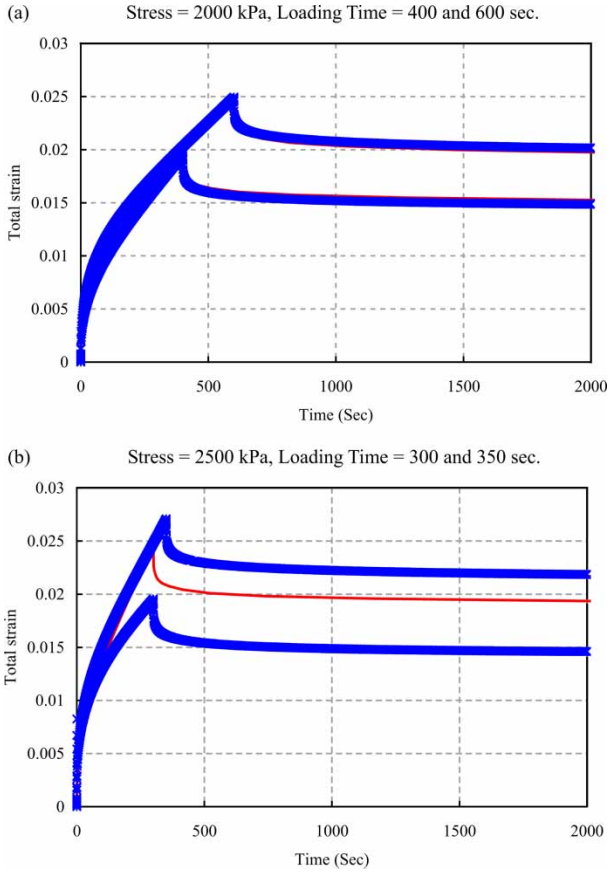

Figure 10. The comparison of total strain between measurements and model predictions at a temperature of 10°C.

Figure 6 in which the viscoplastic parameters at different temperatures are listed in Table 4.

4.3 *Numerical predictions of experimental measurements*

Once the viscoelastic material parameters (D_n, λ_n, g_1 and g_2) and the viscoplastic material parameters (Γ, N, σ_y^0, κ_0, κ_1, κ_2, α and β) are determined, then the UMAT subroutine in the FE code ABAQUS (2008) is used to calculate the creep-recovery response and compare the results with the experimental measurements. The FE model considered here is simply a three-dimensional single element (C3D8R), which is used to obtain the response due to creep-recovery loading. Figure 7 shows a comparison between the experimental data and the predictions for the total strain at a temperature of 20°C. Figures 8 and 9 show comparisons of the decoupled viscoelastic and viscoplastic strain components with the model predictions at a temperature of 20°C, respectively. Good predictions are obtained for the total, viscoelastic and viscoplastic strain. Figures 10 and 11 show the comparison of total strain between experimental measurements and predictions at temperatures 10 and 40°C, respectively, where again reasonable agreements are obtained. The predictions deviate from the experimental data for the cases: (1) stress level = 1500 kPa for LT = 420 s at a temperature of 20°C, (2) stress level = 2500 kPa for LT = 300 s at a temperature of 10°C and (3) stress level = 500 kPa for LT = 180 s at a temperature of 40°C. By looking at the experimental measurements of these cases (Figures 7(b), 10(b) and 11(a)), the responses are deviant as compared with the other measurements at the same stress level and temperature. Generally, the creep response for different LT should follow the same curve, which is not the case in these reported experiments. Hence, the FE predictions deviate from the measurements for these cases and it will be very difficult to get closer predictions of the creep-recovery experimental data. Therefore, more accurate and cleaner experimental data are desirable to fully validate the presented model, which is the scope of the current work by the authors.

Moreover, the FE model with the calibrated material parameters is used to analyse the material response at different temperatures. The simulated case involves a step-

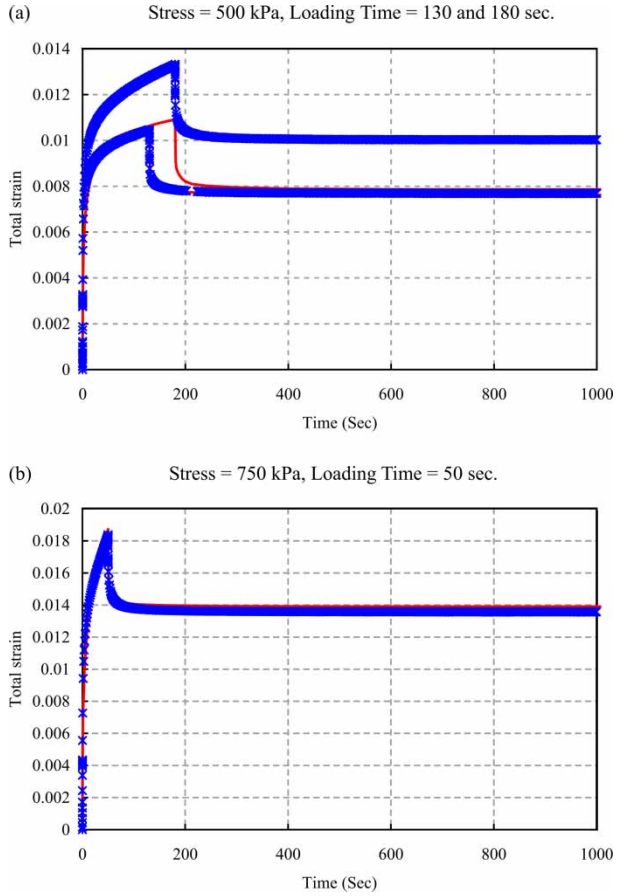

Figure 11. The comparison of total strain between measurements and model predictions at a temperature of 40°C.

loading applying a stress level of 500 kPa for 180 s. The comparison of the resulted material response is shown in Figure 12. This figure shows that increasing the temperature increases the total, viscoelastic and viscoplastic strains, which is expected. Figure 13 shows the viscoelastic and viscoplastic parts of the total strain for different temperatures as compared to the experimental data. This figure shows that increasing the temperature from 10 to 40°C increases the viscoplastic portion from 60 to 70%, whereas the viscoelastic portion decreases from 40 to 30%. Moreover, the percentage of the viscoelastic strain decreases with an increase in the LT; while the portion of viscoplastic strain increases with the LT. Also, the results indicate that the viscoplastic component dominates the material response at higher temperatures, whereas the viscoelastic component is more important at lower temperatures.

The constitutive model reported in this paper does not consider damage evolution for more accurate representation of the nonlinear behaviour of asphalt concrete mixes. This will be incorporated within the framework of continuum damage mechanics where damage due to both

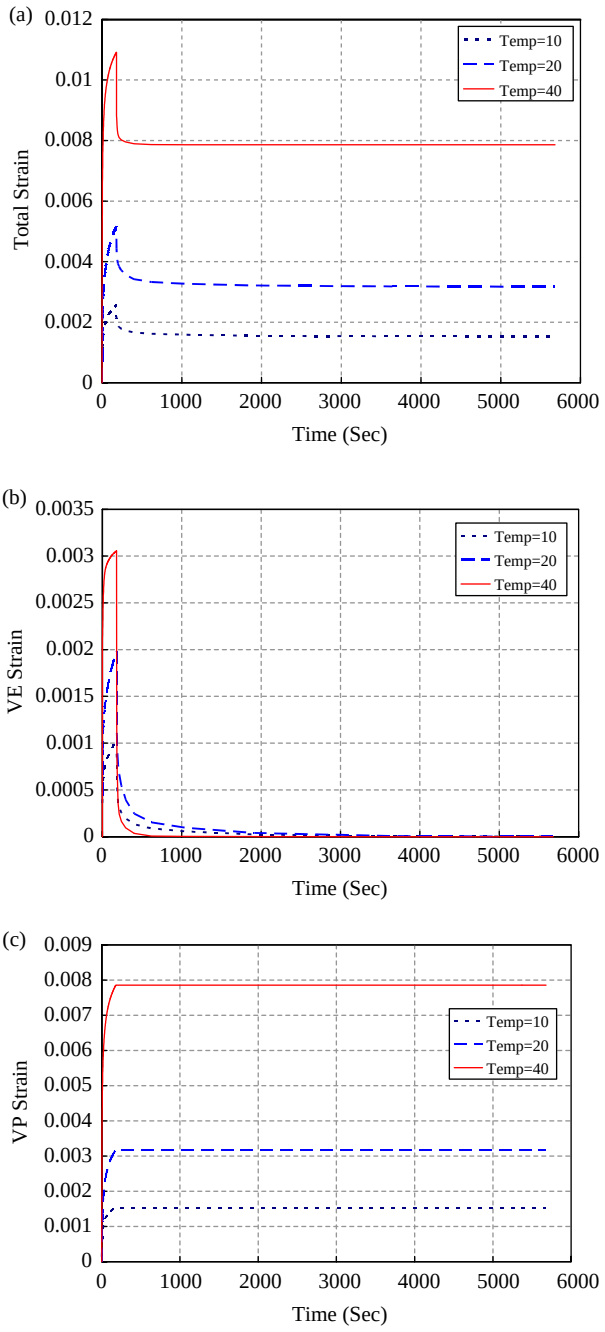

Figure 12. The comparison of material response at different temperatures (in °C) for (a) total strain, (b) viscoelastic strain and (c) viscoplastic strain.

mechanical and environmental (e.g. moisture) loading conditions will be considered.

5. Conclusions

The focus of this study is on the coupling of nonlinear viscoelasticity and viscoplasticity for modelling the nonlinear behaviour of asphalt concrete mixes. The

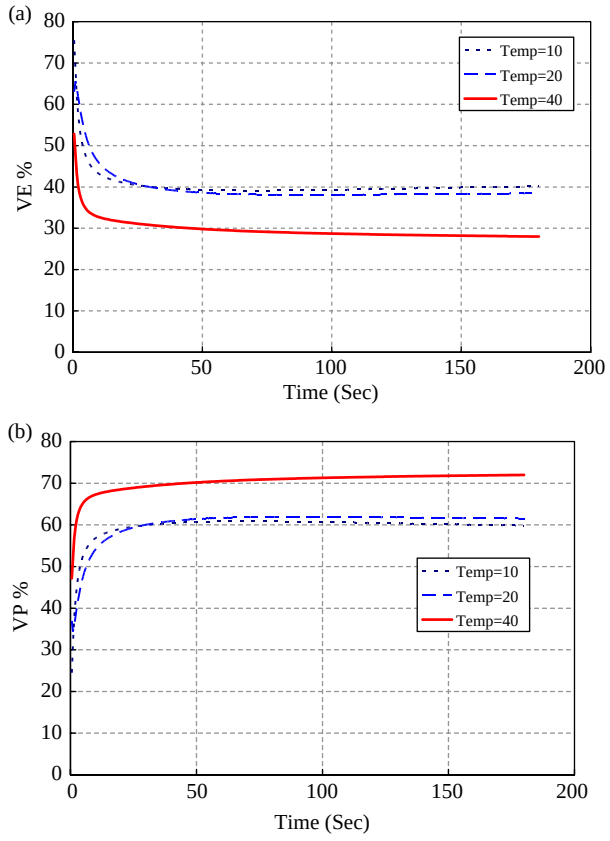

Figure 13. The comparison at different temperatures (in °C) for (a) the viscoelastic strain percentage and (b) the viscoplastic strain percentage.

computational algorithm necessary to enhance this coupling is developed and validated against a set of creep-recovery experimental data for different constant stress levels and different temperatures. A systematic calibration procedure is proposed for identifying the material parameters associated with the nonlinear viscoelastic model and the viscoplastic model. The results from the experimental analysis show that the viscoelastic strain component exhibits a nonlinear response, which justifies the need for a nonlinear viscoelastic model, particularly, at high-stress levels and temperatures. The viscoplastic parameters are identified by separating the viscoelastic and viscoplastic strain components. The viscoplastic analysis indicated that the overstress function in Perzyna model should be modified by normalising it with respect to the stress to incorporate the applied stress effect on the viscoplastic yield surface. The analysis also shows that the viscosity parameter Γ increases with increasing temperature, whereas the viscoplasticity isotropic hardening parameters decrease with decreasing temperature. In fact, the experimental analyses indicate that a viscoplastic model different than the Perzyna viscoplasticity could be necessary to model the viscoplastic response of asphaltic mixes.

The constitutive model is validated by comparing the FE results with experimental measurements at different combinations of temperatures and stress levels, and the results show that the model predictions have good agreements with the experimental measurements. Moreover, the numerical simulations at different temperatures show that increasing the temperature will increase the percentage of the viscoplastic strain, but decrease the percentage of the viscoelastic strain from the total strain. This result indicated that the viscoelastic response controls the material behaviour at lower temperatures, and the viscoplastic response dominates the material behaviour at higher temperatures. Moreover, the presented results illustrate that the model can explain the material behaviour at different temperatures, different stress levels and different LT.

The present analysis only considers the creep-recovery test and it is, therefore, needed to analyse more different tests to fully validate the present constitutive model such as the triaxial test and the uniaxial constant strain rate test to obtain the viscoplastic properties individually. Moreover, the lowest stress level at each temperature, which is used in this study for identifying the material constants associated with linear viscoelasticity, could have induced a nonlinear viscoelastic behaviour. Therefore, it is needed to conduct the test at small stress levels and temperatures to accurately identify the linear viscoelastic material parameters. Also, future work will focus on coupling the presented nonlinear viscoelastic and viscoplastic model with a continuum damage mechanics framework.

References

ABAQUS, 2008. *Version 6.8*. Providence, RI: Habbit, Karlsson and Sorensen, Inc.

Christensen, R.M., 1968. On obtaining solutions in nonlinear viscoelasticity. *Journal of Applied Mechanics*, 35, 129–133.

Collop, A.C., *et al.*, 2003. *Development and finite element implementation of stress-dependent elastoviscoplastic constitutive model with damage for asphalt*. Transportation Research Record 1832. Washington, DC: Transportation Research Board, 96–104.

Dessouky, S., 2005. *Multiscale approach for modeling hot mix asphalt*. Dissertation (PhD). Texas A&M University, College Station, TX.

Grenfell, J.R.A., *et al.*, 2008. Deformation characterization of asphalt concrete behaviour. *Journal of the Association of Asphalt Paving Technologists*, 77, 479–516.

Haj-Ali, R.M. and Muliana, A.H., 2004. Numerical finite element formulation of the Schapery non-linear viscoelastic material model. *International Journal for Numerical Methods in Engineering*, 59, 25–45.

Huang, C.W., *et al.*, 2007. Nonlinear viscoelastic analysis of asphalt mixes subjected to shear loading. *Mechanics of Time Dependent Materials*, 11, 91–110.

Kim, Y., Allen, D.H. and Little, D.N., 2007. Computational constitutive model for predicting nonlinear viscoelastic

damage and fracture failure of asphalt concrete mixtures. *International Journal of Geomechanics*, 7, 102–110.

Kose, S., *et al.*, 2000. *Distribution of strains within hot-mix asphalt binders*. Transportation Research Record 1728. Washington, DC: Transportation Research Board, 21–27.

Lai, J. and Bakker, A., 1996. 3D schapery representation of non-linear viscoelasticity and finite element implementation. *Computational Mechanics*, 18, 182–191.

Lee, H.J. and Kim, Y.R., 1998. A uniaxial viscoelastic constitutive model for asphalt concrete under cyclic loading. *Journal of Engineering Mechanics*, 124, 32–40.

Lemaitre, J. and Chaboche, J.-L., 1990. *Mechanics of solid materials*. London: Cambridge University Press.

Lu, Y. and Wright, P.J., 1998. Numerical approach of visco-elastoplastic analysis for asphalt mixtures. *Journal of Computers and Structures*, 69, 139–157.

Masad, E. and Somadevan, N., 2002. Microstructural finite-element analysis of influence of localized strain distribution of asphalt mix properties. *Journal of Engineering Mechanics*, 128, 1105–1114.

Masad, E., *et al.*, 2005. Viscoplastic modeling of asphalt mixes with the effects of anisotropy, damage, and aggregate characteristics. *Journal of Mechanics of Materials*, 37, 1242–1256.

Masad, E., Dessouky, S. and Little, D., 2007. Development of an elastoviscoplastic microstructural-based continuum model to predict permanent deformation in hot mix asphalt. *International Journal of Geomechanics*, 7, 119–130.

Perl, M., Uzan, J. and Sides, A., 1983. *Visco-elasto-plastic constitutive law for bituminous mixture under repeated loading*. Transportation Research Record 911. Washington, DC: Transportation Research Board, 20–26.

Perzyna, P., 1971. Thermodynamic theory of viscoplastcity. *Advances in Applied Mechanics*, 11, 313–354.

Saadeh, S., Masad, E. and Little, D., 2007. Characterization of hot mix asphalt using anisotropic damage viscoelastic-viscoplastic model and repeated loading. *Journal of Materials in Civil Engineering*, 19 (10), 912–924.

Sadd, M.H., Parameswaran, D.Q. and Shukla, A., 2004. *Simulation of asphalt materials using finite element micromechanical model with damage mechanics*. Transportation Research Record 1832. Washington, DC: Transportation Research Board, 86–95.

Schapery, R.A., 1969. On the characterization of nonlinear viscoelastic materials. *Polymer Engineering and Science*, 9, 295–310.

Schapery, R.A., 1991. Simplifications in the behavior of viscoelastic composites with growing damage. *In*: *Proceedings of the IUTAM symposium on inelastic deformation of composite materials*. Berlin: Springer Verlag.

Schapery, R.A., 2000. Nonlinear viscoelastic solids. *International Journal of Solids and Structures*, 37, 359–366.

Seibi, A., *et al.*, 2001. *Constitutive relations for asphalt concrete under high rates of loading*. Transportation Research Record 1767. Washington, DC: Transportation Research Board, 111–119.

Sides, A., Uzan, J. and Perl, M., 1985. A comprehensive visco-elastoplastic characterization of sand-asphalt under compression and tension cyclic loading. *Journal of Testing and Evaluation*, 13, 49–59.

Tashman, L., *et al.*, 2005. Microstructural viscoplastic continuum model for asphalt pavements. *Journal of Engineering Mechanic*, 131 (1), 48–57.

Touati, D. and Cederbaum, G., 1998. Post buckling of nonlinear viscoelastic imperfect laminated plates. Part I: material considerations. *Composite Structures*, 42, 33–41.

Wang, W.M., Sluys, L.J. and de Borst, R., 1997. Viscoplasticity for instabilities due to strain softening and strain-rate softening. *International Journal for Numerical Methods in Engineering*, 40, 3839–3864.